CHEMPHYSCHEM

DOI: 10.1002/cphc.200700709

Proton and Deuteron Transfer Reactions in Molecular Nanoclusters

Hyojoon Kim*[a] and Raymond Kapral*[b]

Proton and deuteron transfer rates and mechanisms are studied in polar molecular nanoclusters. The cluster environment strongly influences the reaction rate and the nature of these changes is studied as a function of the cluster size. The stabilities of the covalent reactant and polar product states change with cluster size and this effect alters both the equilibrium properties and transfer rate. The proton and deuteron are light quantum particles and the quantum character of the rate process is reflected in the magnitude of the kinetic isotope effect. Our mixed quantum–classical rate simulations indicate that the magnitude of the isotope effect decreases as the cluster size increases. More generally, our study shows how quantum effects combined with structural nanosolvation effects can lead to changes in reaction rates and mechanisms which should be applicable to many quantum charge transfer reactions in molecular nanoclusters.

1. Introduction

Nanometer-scale materials typically have a very high surface/volume ratio[1,2] and, as a consequence, effects due to surface forces often play an essential role in determining the equilibrium and dynamical properties of such materials. Surface forces are especially important in molecular nanoclusters, which bridge the gap between molecular entities and bulk phase materials,[2] and this feature has stimulated both experimental and theoretical studies of cluster systems.[3] Molecular clusters can serve as distinctive environments for chemical reactions, which often take place with mechanisms and rates that differ significantly from their bulk phase analogs. Such molecular cluster reactions are important in atmospheric chemistry where many reactions take place in nano and micron-sized water or other molecular droplets.[4] Similarly, in microemulsions, chemical reactions may take place in nanodroplets that contain only a few molecules of the reactive species.[5,6]

Herein we investigate a particular class of reactions that involve the transfer of a proton between two molecular groups in a molecular complex dissolved in a polar molecular nanocluster. Proton transfer reactions are involved in many chemical and biological processes[7–11] and there have been numerous experimental and computational studies of proton transfer in nano-environments such as nano-confined materials[12–15] and nanoclusters.[16–24] While it is possible to approximate the dynamics of the polar molecules comprising the cluster environment by classical mechanics, the proton and its interactions with the polar solvent molecules must be treated using quantum dynamics. Consequently, our investigations of this system employ mixed quantum-classical dynamics.[25] The use of such a method allows us to study the mechanisms as well as the rates of this important class of quantum mechanical reactions. Both of these aspects of the quantum reaction are influenced by the nanocluster environment.[26]

The quantum mechanical character of proton transfer reactions may be verified experimentally by observing the magnitude of the kinetic isotope effect (KIE).[27–31] A large KIE was found in experimental studies of excited-state proton transfer reactions in clusters.[20,21] We pose the question, can the small size of nanomaterials strongly affect the magnitude of the kinetic isotope effect? To answer this question here, we apply our recently-developed quantum-classical methods[31–33] to investigate quantum proton and deuteron transfer rates in polar nanoclusters.

2. Model and Methods

We consider a simplified model describing proton transfer in a hydrogen-bonded phenol-trimethylamine complex as in Equation (1)

$$PhO{-}H\cdots N(CH_3)_3 \rightleftharpoons PhO^- \cdots H{-}N(CH_3)_3^+ \qquad (1)$$

dissolved in a cluster of rigid methyl chloride molecules.[34] This model has often been used to study quantum effects on proton transfer rates in the condensed phase since it captures many generic features of proton transfer in polar environments.[14,15,35–41] Due to hydrogen bonding, the complex can exist in the covalent A (left) and ionic B (right) forms shown in Equation (1). The covalent state is more stable in the gas

[a] *Prof. H. Kim*
Department of Chemistry
Dong-A University
Hadan-2-dong, Busan 604-714 (Korea)
Fax: (+82) 51-200-7259
E-mail: hkim@chem.utoronto.ca

[b] *Prof. R. Kapral*
Chemical Physics Theory Group
Department of Chemistry, University of Toronto
Toronto, Ontario M5S 3H6 (Canada)
Fax: (+1) 416-978-5325
E-mail: rkapral@chem.utoronto.ca

phase while the ionic state is more stable in a polar solvent. In contrast to bulk phase systems, when proton transfer takes place in a nanocluster, the entire cluster can reorganize its structure in order to achieve favorable solvation for the ionic or covalent states: the ionic state of the molecular complex tends to occupy a position in the center of the cluster to maximize the solvation effects while the covalent state of the complex tends to lie on the cluster surface (see Figure 1).

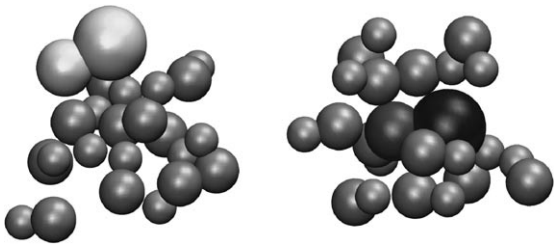

Figure 1. Two representative cluster configurations for the covalent (left) and ionic (right) states.

The complex and the CH_3Cl molecules are heavy and may be treated classically to a good approximation; the proton or deuteron must be treated quantum mechanically. The total Hamiltonian of the systems is given by Equation (2)

$$H(q,X) = P^2/(2\,\mathrm{M}) + H_{\mathrm{qm}}(q,R) \tag{2}$$

where $X=(R,P)$ represents the positions and momenta of the classical particles and H_{qm} includes the kinetic energy of the quantum particle and all interaction potentials. The proton coordinate is denoted by q. It is convenient to work in an adiabatic basis when following the quantum evolution of the proton transfer process. The adiabatic wavefunctions $\psi_\alpha(q;R)$ are the solutions of the Schrödinger equation [Eq. (3)],

$$H_{\mathrm{qm}}(q,R)\psi_\alpha(q;R) = E_\alpha(R)\psi_\alpha(q;R) \tag{3}$$

where $E_\alpha(R)$ is the energy of the α protonic state for a fixed configuration R of the classical particles. In our simulations, the wavefunction $\psi_\alpha(q;R)$ is written as a superposition of harmonic oscillator basis functions in Equation (4)[35,41]

$$\psi_\alpha(q;R) = \sum_i c_{i\alpha}(R)\phi_i(q) \tag{4}$$

where [Eq. (5)]

$$\phi_i(q) = \left(2^m m!\sqrt{\pi}/b\right)^{-1/2} H_m(b(q-q_0))e^{-b^2(q-q_0)^2/2} \tag{5}$$

with H_m a Hermite polynomial. We have used 12 basis functions with $q_0=0.048$ Å and -0.552 Å and $m=0$–5. We let $b=7.732$ Å^{-1} and $b=9.195$ Å^{-1} for the proton and deuteron, respectively.

A convenient choice of reaction coordinate for proton transfer processes is the solvent polarization ΔE, which is defined as the solvent potential difference between two points s and s' within the complex corresponding to the minima of the gas-phase potential [Eq. (6)],[41–44]

$$\Delta E(R) = \sum z_i e\left(\frac{1}{|R_i - s|} - \frac{1}{|R_i - s'|}\right) \tag{6}$$

Here $z_i e$ is the charge on atom i. The free energy along the reaction coordinate for a nanocluster with N_s solvent molecules and the proton in state α, $W_\alpha(\Delta E';N_s)$, may be defined as in Equation (7)[41]

$$\beta W_\alpha(\Delta E;N_s) = -\ln\frac{\langle\delta(\Delta E(R)-\Delta E)\rangle_\alpha}{P_u(N_s)} - \ln\frac{p_\alpha}{p_1} \tag{7}$$

where $\langle\cdots\rangle_\alpha = \int dX\cdots e^{-\beta H_\alpha}/\int dX e^{-\beta H_\alpha}$, p_α is the probability that the system is in state α, β is the inverse temperature and $P_u(N_s)$ is a uniform probability density. The quantity ΔE without an argument refers to a numerical value of this quantity. We have computed the free energy $\beta W_\alpha(\Delta E;N_s)$ by sampling from long adiabatic ground-state trajectories. The equilibrium constant $K_{\mathrm{eq}}=[B]/[A]$ is related to the free energy by Equation (8)

$$K_{\mathrm{eq}} = \int_{\Delta E^\ddagger}^{\infty} d\Delta E e^{-\beta W_1(\Delta E)} \Big/ \int_{-\infty}^{\Delta E^\ddagger} d\Delta E e^{-\beta W_1(\Delta E)} \tag{8}$$

where $\Delta E^\ddagger$ is a dividing surface along the reaction coordinate. The rate coefficient can be calculated from the reactive flux correlation function in Equation (9)[45,33]

$$k_{AB}(t) = Z_R^{-1}\sum_\alpha \int dX \mathrm{Re}\left[N_B^{\alpha\alpha}(X,t)\right] \times \Delta\dot{E}(R)\delta(\Delta E(R)-\Delta E^\ddagger)e^{-\beta H_\alpha(X)} \tag{9}$$

where Z_R denotes the reactant partition function. The nonadiabatic evolution of the species variable operator $\hat{N}_B = \theta(\Delta E(R)-\Delta E^\ddagger)$ was computed using quantum-classical Liouville dynamics[46] using methods described elsewhere.[26] The liquid-state clusters of the complex and N_s solvent molecules were prepared by melting face-centered cubic lattice structures. The sequential short time propagation algorithm,[47] which represents the quantum-classical Liouville evolution in terms of an ensemble of surface-hopping trajectories, was used for the nonadiabatic dynamics of the transfer process, and classical trajectory segments that enter this algorithm were integrated using the velocity Verlet algorithm.[48] The rate coefficients were obtained from averages over 2×10^4 trajectories with a time step $\Delta t=5$ fs and with the constraint $\Delta E=\Delta E^\ddagger$ imposed for initial sampling.

3. Results and Discussion

In Figure 2, we show how the free energy along the polarization reaction coordinate ΔE depends on the size of the cluster N_s for the ground and the first excited states of the deuteron at $T=150$ K. We set $P_u=1$ at $N_s=8$ to fix the scale of the plot. The ground-state surface has a double-well form where the minima correspond to the covalent and ionic states, while the

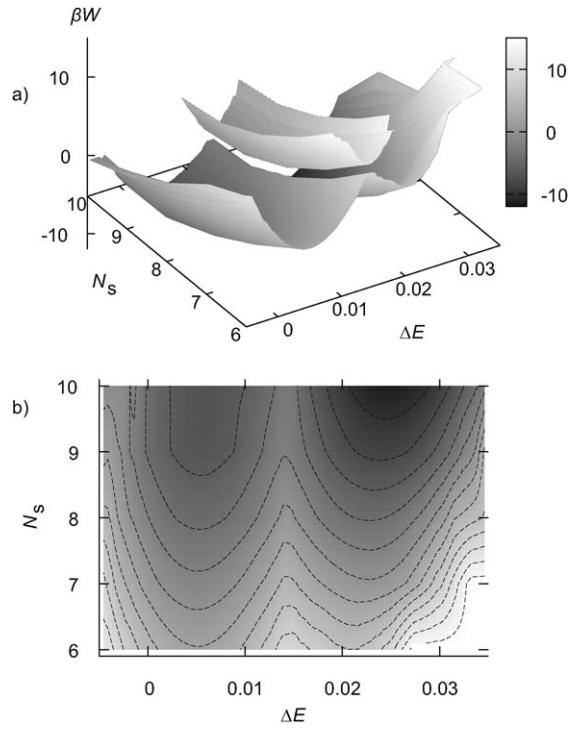

Figure 2. a) Three-dimensional free energy profiles (βW) of ground and excited states as a function of the reaction coordinate ΔE and the cluster size N_s at $T=150$ K for the deuteron transfer. b) Two-dimensional contour plot of ground-state free energy with the same shading as in (a).

excited-state surface has a single-well form with its minimum located at the barrier top of the ground-state free energy. The shapes of ground- and excited-state surfaces for $N_s=8$ are shown in Figure 3a, where one can see a typical avoided crossing between adiabatic states. The solid lines are fits to covalent and ionic states. The contour plot in Figure 2b shows that the stability between the covalent and ionic states is reversed as N_s increases, with the ionic state being favored in a large cluster. We also found that the position of the ionic state minimum

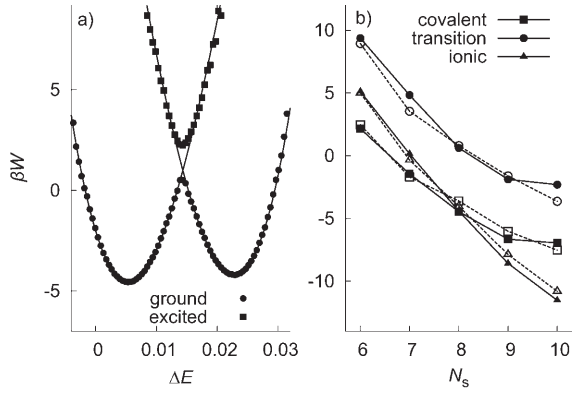

Figure 3. a) Ground- and excited-state free energy profiles for the deuteron transfer with $N_s=8$ at $T=150$ K. Parabolic fits to two ground state free energy minima are indicated by solid lines. b) Plots of the minima of the covalent and ionic states, and maxima of the transition state between them, as a function of N_s for the proton (○) and deuteron (●) transfer reactions.

depends on N_s more strongly than either the covalent state minimum or the barrier top position. The energy gap between ground and excited states at the barrier top was found to be very weakly dependent on N_s.

The solvation of the complex becomes stronger with an increasing number of polar cluster solvent molecules. A quantitative measure of the solvation strength is shown in Figure 3b where the free energies of the ionic and covalent states, and the transition state between them, is plotted as a function of N_s. As N_s increases, all states are stabilized but the stabilization of the ionic state is greater than that of the covalent state. As a result, the covalent state is more stable for $N_s<7$ while the ionic state is more stable for larger clusters.

The equilibrium constant was calculated using Equation (8). In Figure 4a, we compare K_{eq} for the proton and deuteron transfer reactions as a function of N_s on a semilog scale. The

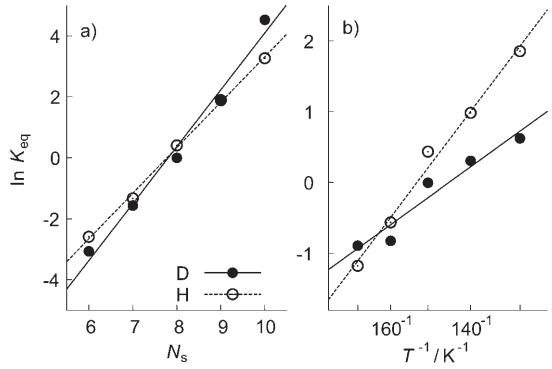

Figure 4. Plots of the equilibrium constant K_{eq} a) as a function of N_s at $T=150$ K and b) as a function of inverse temperature $1/T$ for $N_s=8$ on a semilog scale for the deuteron (●) and proton (○) transfers.

Figure shows that the solvation free energy per solvent molecule is 2.5 kJ mol^{-1} for the deuteron and 1.9 kJ mol^{-1} for the proton. This implies that the deuteron complex is more strongly influenced by solvation in the cluster. This can be understood as follows. Due to its larger mass, the distribution of the deuteron probability density is narrower than that of the proton. This can be seen in Figure 5 where sample probability

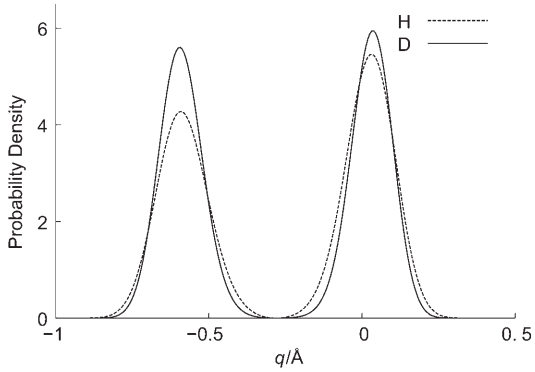

Figure 5. Ground state probability density distribution along the one-dimensional proton and deuteron coordinate q for the same cluster configuration.

densities for the proton and deuteron are plotted for the same cluster environment. The broader proton probability density results in a weaker solvation of the proton complex than that for the deuteron complex when the cluster size (N_s) increases. In Figure 4a, we can see that the magnitudes of equilibrium constants for the proton and deuteron transfer reactions are reversed as N_s increases due to the difference between the solvation strengths of a cluster solvent molecule for either the proton or the deuteron. As a result, the relative stability of the covalent deuteron complex is larger than that of the corresponding proton complex for small cluster systems, while it is smaller for large clusters. The difference in probability densities also makes the equilibrium constant for the deuteron complex less dependent on the temperature, as seen in Figure 4b. These results both show that the covalent state is preferred over the ionic state at higher temperatures. The slope determined from this plot is $-7.7\ \mathrm{kJ\,mol^{-1}}$ for the deuteron, while it is $-14\ \mathrm{kJ\,mol^{-1}}$ for the proton. The deuteron transfer reaction is also less exothermic than the proton-transfer reaction.

The kinetic isotope effect, which is often used to gauge the magnitude of quantum mechanical effects, is defined as the ratio of the proton to deuteron rate constants, namely, $\mathrm{KIE} = k^{P}_{AB}/k^{D}_{AB}$. The rate constants k_{AB} were determined from the long-time plateau value of $k_{AB}(t)$. The transition state theory (TST) rate constant was determined from the initial value of the time dependent rate coefficient, namely, $k^{TST}_{AB} = k_{AB}(0^{+})$. The small energy gap near the barrier top implies that nonadiabatic transitions may affect the transfer dynamics. We find that significant nonadiabatic effects are present and approximately 35% of all trajectories experience at least one nonadiabatic transition. However, the rate constants are not affected significantly by nonadiabatic effects. Since the nonadiabatic coupling depends on the momentum and therefore the temperature, the relatively low temperature of our nanocluster systems makes the nonadiabatic contributions to the rate small.

In Figure 6 we plot the KIE for the rate constants k_{AB} and k^{TST}_{AB} as functions of N_s and T. For both k_{AB} and k^{TST}_{AB}, the general trends of the dependence of the KIE on N_s and T are similar but the magnitude of the KIE for k_{AB} is larger than that for k^{TST}_{AB}. This indicates the importance of dynamic recrossing of the barrier top. The KIE value was found to depend very strongly on the cluster size, showing that the quantum effects on the transfer rates are stronger for smaller clusters. The dependence of the KIE on T is relatively weak and it tends to a small value at a high temperatures. The TST rate constant k^{TST}_{AB} depends on the barrier height and the reactant (covalent state) well frequency. We observe that the reactant well frequency of proton is similar to that of deuteron and the KIE for k^{TST}_{AB} is governed by the difference in barrier heights.

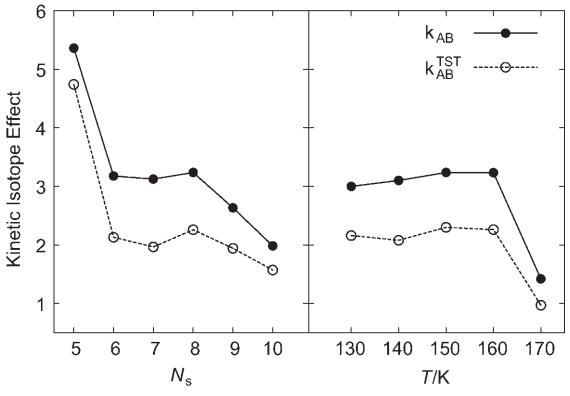

Figure 6. Kinetic isotope effect determined from nonadiabatic, k_{AB}, and TST, k^{TST}_{AB}, rate coefficients for various values of N_s at $T = 150$ K (left) and for $N_s = 8$ at various temperatures (right).

In Figure 7, we show how the barrier heights of the proton and deuteron transfer reactions depend on N_s and T. The trends are similar for deuteron and proton transfer reactions and both show that the barrier heights decrease with increases in N_s. The barrier height in dimensionless units (βW) depends weakly on T. At $T = 170$ K, the difference in barrier heights is small and this is responsible for the reduction of the TST kinetic isotope effect to a value near unity at this temperature. Since quantum effects are more manifest at lower temperatures, the small difference between barrier heights at high temperatures is expected. Thus, we find that the strong dependence of the KIE on the cluster size arises from quantum effects in both the dynamics and equilibrium structure. We can see the former effects in the difference between KIE determined from k_{AB} and k^{TST}_{AB}, since dynamic recrossing contributions to the rate are affected by the quantum mechanical character of proton and deuteron. The latter effects are seen in the difference of free energy barrier heights.

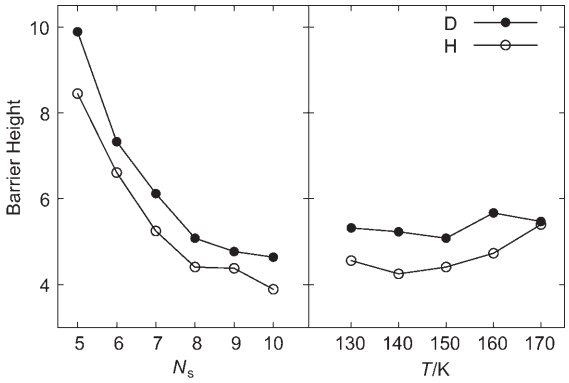

Figure 7. The dimensionless barrier height for proton (○) and deuteron (●) transfer reactions for the passage from the covalent to the ionic state for various values of N_s at $T = 150$ K (left) and for $N_s = 8$ at various temperatures (right).

4. Conclusions

The quantum-classical dynamical simulations of proton and deuteron transfer reactions have shown how quantum mechanical aspects of the reaction are affected by the peculiar nature of the nanocluster environment. The stabilities of proton and deuteron complex states are strongly influenced by the solvation strength, making these transfer reactions in nanoclusters distinct from their counterparts in the bulk phase. By analyzing the dependence of the free energy on the

number of cluster solvent molecules and the temperature, we found that the relative stabilities of the covalent and ionic states for both proton and deuteron transfer reactions are reversed as the cluster size or the temperature increases. The difference in the proton and deuteron masses affects the quantum mechanical probability densities and this, in turn, influences the solvation strength of surrounding cluster molecules. Consequently, the magnitude of the equilibrium constant and the relative stability of the covalent and ionic states show different dependencies on the cluster size. While an ionic deuteron complex is more stable than that of a proton in a large cluster, it may be less stable in a small cluster due to the difference in the solvation strengths.

The analysis of the quantum-classical transition state theory reaction rates shows that the kinetic isotope effect strongly depends on the difference of activation barrier heights caused by the different quantum characters of proton and deuteron. The quantum-classical dynamic recrossing of the dividing surface between covalent and ionic states also affects the kinetic isotope effect. Nonadiabatic transitions between the protonic ground and excited states occur more frequently in the deuteron transfer than in the proton transfer, but the transfer rates are weakly influenced by nonadiabatic transitions because of the relatively low temperatures in our systems. As a result, adiabatic dynamics provides a good approximation for the predictions of the transfer rates. Our investigations should provide insight into how quantum effects in conjunction with structural nanosolvation effects can lead to changes in reaction rates and mechanisms. The basic elements in our study should be applicable to many quantum charge-transfer reactions in molecular nanoclusters.

Acknowledgements

This work was supported in part by a grant from the Natural Sciences and Engineering Research Council of Canada.

Keywords: charge transfer · cluster compounds · isotope effects · molecular dynamics · reaction mechanisms

[1] G. A. Ozin, A. Arsenault, *Nanochemistry: A Chemical Approach to Nanomaterials*, RSC, Cambridge, **2005**.
[2] F. Baletto, R. Ferrando, *Rev. Mod. Phys.* **2005**, *77*, 371–423.
[3] H. S. Nalwa, *Encyclopedia of Nanoscience and Nanotechnology*, American Scientific, New York, **2004**.
[4] B. J. Gertner, J. T. Hynes, *Science* **1996**, *271*, 1563–1566.
[5] V. K. Vanag, I. R. Epstein, *Phys. Rev. Lett.* **2001**, *87*, 228301.
[6] I. R. Epstein, *Science* **2007**, *315*, 775–776.
[7] T. Elsaesser, H. J. Bakker, *Ultrafast Hydrogen Bonding Dynamics and Proton Transfer Processes in the Condensed Phase*, Kluwer, Dordrecht, **2002**.
[8] S. J. Benkovic, S. Hammes-Schiffer, *Science* **2003**, *301*, 1196–1202.
[9] M. Garcia-Viloca, J. Gao, M. Karplus, D. G. Truhlar, *Science* **2004**, *303*, 186–195.
[10] J. T. Hynes, J. P. Klinman, H.-H. Limbach, R. L. Schowen, *Hydrogen-Transfer Reactions*, Wiley-VCH, Weinheim, **2007**.
[11] J. T. Hynes, *Nature* **2007**, *446*, 270–272.
[12] B. Cohen, D. Huppert, K. M. Solntsev, Y. Tsfadia, E. Nachliel, M. Gutman, *J. Am. Chem. Soc.* **2002**, *124*, 7539–7547.
[13] O. H. Kwon, D. J. Jang, *J. Phys. Chem. B* **2005**, *109*, 8049–8052.
[14] S. M. Li, W. H. Thompson, *J. Phys. Chem. B* **2005**, *109*, 4941–4946.
[15] W. H. Thompson, *J. Phys. Chem. B* **2005**, *109*, 18201–18208.
[16] J. Steadman, J. A. Syage, *J. Chem. Phys.* **1990**, *92*, 4630–4632.
[17] J. A. Syage, J. Steadman, *J. Chem. Phys.* **1991**, *95*, 2497–2510.
[18] R. Knochenmuss, G. R. Holtom, D. Ray, *Chem. Phys. Lett.* **1993**, *215*, 188–192.
[19] S. K. Kim, J. K. Wang, A. H. Zewail, *Chem. Phys. Lett.* **1994**, *228*, 369–378.
[20] J. A. Syage, *J. Phys. Chem.* **1995**, *99*, 5772–5786.
[21] S. K. Kim, J. J. Breen, D. M. Willberg, L. W. Peng, A. Heikal, J. A. Syage, A. H. Zewail, *J. Phys. Chem.* **1995**, *99*, 7421–7435.
[22] M. Meuwly, A. Bach, S. Leutwyler, *J. Am. Chem. Soc.* **2001**, *123*, 11446–11453.
[23] M. Meuwly, M. Karplus, *J. Chem. Phys.* **2002**, *116*, 2572–2585.
[24] A. Bach, C. Tanner, C. Manca, H. M. Frey, S. Leutwyler, *J. Chem. Phys.* **2003**, *119*, 5933–5942.
[25] R. Kapral, *Annu. Rev. Phys. Chem.* **2006**, *57*, 129–157.
[26] H. Kim, R. Kapral, *J. Chem. Phys.* **2006**, *125*, 234309.
[27] J. K. Hwang, A. Warshel, *J. Am. Chem. Soc.* **1996**, *118*, 11745–11751.
[28] S. Lee, J. T. Hynes, *J. Chim. Phys. PCB* **1996**, *93*, 1783–1807.
[29] A. Kohen, J. P. Klinman, *Acc. Chem. Res.* **1998**, *31*, 397.
[30] L. I. Krishtalik, *Biochim. Biophys. Acta Bioenerg.* **2000**, *1458*, 6–27.
[31] H. Kim, G. Hanna, R. Kapral, *J. Chem. Phys.* **2006**, *125*, 084509.
[32] H. Kim, R. Kapral, *J. Chem. Phys.* **2005**, *122*, 214105.
[33] H. Kim, R. Kapral, *J. Chem. Phys.* **2005**, *123*, 194108.
[34] H. Azzouz, D. Borgis, *J. Chem. Phys.* **1993**, *98*, 7361–7375.
[35] S. Hammes-Schiffer, J. C. Tully, *J. Chem. Phys.* **1994**, *101*, 4657–4667.
[36] D. Antoniou, S. D. Schwartz, *J. Chem. Phys.* **1999**, *110*, 465–472.
[37] D. Antoniou, S. D. Schwartz, *J. Chem. Phys.* **1999**, *110*, 7359–7364.
[38] R. P. McRae, G. K. Schenter, B. C. Garrett, Z. Svetlicic, D. G. Truhlar, *J. Chem. Phys.* **2001**, *115*, 8460–8480.
[39] S. Y. Kim, S. Hammes-Schiffer, *J. Chem. Phys.* **2003**, *119*, 4389–4398.
[40] T. Yamamoto, W. H. Miller, *J. Chem. Phys.* **2005**, *122*, 044106.
[41] G. Hanna, R. Kapral, *J. Chem. Phys.* **2005**, *122*, 244505.
[42] A. Warshel, *J. Phys. Chem.* **1982**, *86*, 2218–2224.
[43] R. A. Marcus, N. Sutin, *Biochim. Biophys. Acta* **1985**, *811*, 265–322.
[44] G. Hanna, R. Kapral, unpublished results.
[45] T. Yamamoto, *J. Chem. Phys.* **1960**, *33*, 281–289.
[46] R. Kapral, G. Ciccotti, *J. Chem. Phys.* **1999**, *110*, 8919–8929.
[47] D. MacKernan, R. Kapral, G. Ciccotti, *J. Phys. Condens. Matter* **2002**, *14*, 9069–9076.
[48] M. P. Allen, D. J. Tildesley, *Computer Simulation of Liquids*, Oxford University Press, Oxford, **1987**.

Received: October 11, 2007
Published online on January 29, 2008

